AGU PUBLICATIONS

Water Resources Research

RESEARCH ARTICLE
10.1002/2016WR019502

Early formation of preferential flow in a homogeneous snowpack observed by micro-CT

Francesco Avanzi[1], Giacomo Petrucci[1], Margret Matzl[2], Martin Schneebeli[2], and Carlo De Michele[1]

[1]Department of Civil and Environmental Engineering, Politecnico di Milano, Milano, Italy, [2]WSL Institute for Snow and Avalanche Research SLF, Davos, Switzerland

Key Points:
- We performed X-ray microtomographic observations of wet-snow metamorphism during controlled continuous melting and melt-freeze events
- Results suggest that wet-snow metamorphism dynamics are highly heterogeneous even in an initially homogeneous snowpack
- Wet-snow metamorphism shows in our experiments two strikingly different patterns of homogeneous and heterogeneous grain growth

Supporting Information:
- Supporting Information S1

Correspondence to:
F. Avanzi,
francesco.avanzi@polimi.it

Citation:
Avanzi, F., G. Petrucci, M. Matzl, M. Schneebeli, and C. De Michele (2017), Early formation of preferential flow in a homogeneous snowpack observed by micro-CT, *Water Resour. Res.*, *53*, 3713–3729, doi:10.1002/2016WR019502.

Received 13 JUL 2016
Accepted 30 MAR 2017
Accepted article online 6 APR 2017
Published online 4 MAY 2017

Abstract We performed X-ray microtomographic observations of wet-snow metamorphism during controlled continuous melting and melt-freeze events in the laboratory. Three blocks of snow were sieved into boxes and subjected to cyclic, superficial heating or heating-cooling to reproduce vertical water infiltration patterns in snow similarly to natural conditions. Periodically, samples were taken at different heights and scanned. Results suggest that wet-snow metamorphism dynamics are highly heterogeneous even in an initially homogeneous snowpack. Consistent with previous work, we observed an increase with time in the thickness of the ice structure, which is a measure of grain size. However, this was coupled with large temporal scatter between consecutive measurements of the specific surface area and of the statistical moments of grain thickness distributions. Because of marked differences in the right tail, grain thickness distributions did not show shape invariance with time, contrary to previous analyses. In our experiments, wet-snow metamorphism showed two strikingly different patterns: homogeneous coarsening superimposed by faster heterogeneous coarsening in areas that were affected by preferential percolation of water. Liquid water movement in snow and fast structural evolution may be thus intrinsically coupled by early formation of preferential flow at local scale. These observations suggest that further experiments are highly needed to fully understand wet-snow metamorphism and infiltration patterns in a natural snowpack.

1. Introduction

Snow is not in thermodynamic equilibrium [*Pinzer and Schneebeli*, 2009], due to its high homologous temperature [*Hagenmuller et al.*, 2014] and high vapor pressure [*Pinzer and Schneebeli*, 2009]. Consequently, metamorphism changes density, specific surface area (SSA), and grain shape and size in general [*Colbeck*, 1982]. This process leads to a dramatic change of the hydraulic properties of snow, comparable to converting fine grained sand to a very coarse sand.

Liquid water is an important driver of snow metamorphism [*Colbeck*, 1973]. Wet-snow metamorphism is different from dry snow metamorphism because of the much faster grain growth rates. The interaction between liquid water and the ice structure causes a strict coupling between wet-snow metamorphism and liquid water movement in snow. A specific feature is the formation of preferential flow paths, that can affect deep lying snow layers [*Colbeck*, 1979; *Marsh and Woo*, 1984a, 1984b, 1985; *Schneebeli*, 1995]. This process is obviously of great importance to water flow and all associated processes such as solute transport [*Waldner et al.*, 2004].

Currently, there is no accepted general theory that explains the coarsening of snow, neither for the isothermal metamorphism nor for wet-snow metamorphism. Since the 1960s, wet-snow metamorphism has been often investigated in laboratory experiments. As an example, *Wakahama* [1968] compared grain evolution in dry, moist [*Fierz et al.*, 2009], and saturated snow and found that grain growth is much more rapid in the last case. Similar experiments were also performed by, e.g., *Raymond and Tusima* [1979] and *Tusima* [1985]. They considered saturated snow samples and observed that the mean grain size of snow increases with time (grain coarsening) according to an approximately linear function; the observed coarsening process is similar to Ostwald ripening [*Raymond and Tusima*, 1979]. An evaluation of the temporal evolution of the grain size distribution showed invariance of shape and that the median diameter of grains is a convenient characteristic size descriptor. Later, *Colbeck* [1986a] argued that the volume of grains increases nonlinearly

with time, whereas he confirmed invariance of grain size distribution with time. To our best knowledge, *Brun* [1989] was the first to systematically investigate wet-snow metamorphism in partially saturated conditions, by using an electromagnetic snow-warming device to create homogeneous samples at different liquid water content (henceforth, θ or LWC, in vol%). Results show that the growth rate of grains depends on θ according to a power law. *Marsh* [1987] is among the few examples of field investigations of wet-snow metamorphism: a nonlinear growth of the mean diameter of grains was observed in arctic snow.

The description of the microstructural evolution during wet conditions is a key to predicting water percolation and runoff timing [*Waldner et al*., 2004; *Wever et al*., 2014], albedo evolution [*Tedesco et al*., 2006; *Dietz et al*., 2012], and snow stability [*Schweizer et al*., 2003; *Mitterer et al*., 2011; *Wever et al*., 2016a]. Indeed, predictions of the dynamics of wet-snow metamorphism using existing observations are included in several numerical models of snow structural evolution for avalanche or hydrologic forecasting [*Bartelt and Lehning*, 2002; *Brun et al*., 1992]. However, existing work on wet-snow metamorphism is mainly focused on saturated or initially homogeneously wet snow samples and on constant temperature conditions, which avoid the occurrence of melt-freeze cycles in snow. These experiments represent idealized conditions compared to field conditions, where variable temperature, variable snow wetness, and melt-freeze cycles are paramount processes [*Marsh*, 1987; *Pfeffer et al*., 1990; *Illangasekare et al*., 1990; *Pfeffer et al*., 1991; *Pfeffer and Humphrey*, 1996]. Experiments in more representative conditions may help to understand wet-snow metamorphism under more realistic situations and therefore improve existing models [*Wever et al*., 2016b].

Here we present the results of three cold laboratory experiments where macroscopic snow blocks were subjected to controlled melt or melt-freeze cycles. The protocol enabled to observe wet-snow metamorphism during vertical, heterogeneous infiltration of water in snow, as it usually occurs under natural conditions. The snow structure was characterized using X-ray microtomography by periodically taking samples from the macroscopic artificial snowpack. From these measurements, we investigated the evolution of the microstructure in time, specifically the SSA and the thickness distribution, which is a measure of grain size. No direct observation of liquid water was attempted during the experiments.

2. Methods

2.1. Experiments

We defined a protocol to induce melt or melt-freeze (Figure 1). Experiments M1 and M2 are two replicas (with different duration) of a melt-only process where snow was kept in isothermal state at 0°C; experiment MF included several melt-freeze cycles.

Three snow blocks were sieved into insulated boxes in a cold laboratory, Figure 1a. The initial dimension of each block was 50 cm $\times$ 50 cm $\times$ 30 cm (length $\times$ width $\times$ height). The upper side of the block was open to the environment, whereas the other sides were thermally isolated by Styrofoam. This experimental geometry mimicked a thermally isolated portion of snowpack subjected to energetic exchanges with the atmosphere. We used nature-identical snow, produced by a Snowmaker [*Schleef et al*., 2014]. Water temperature in the heated reservoir of the Snowmaker was set to $+30$°C; air temperature in the cold room was set to -20°C $\pm$ 2°C. This setting produces fresh snow with density around 115–150 kg/m^3, initial SSA around 65 m^2/kg, and classification number equal to C1f/G6 [*Schleef et al*., 2014]. After sieving, each block was left in a cold chamber in subfreezing conditions for 13 (M1), 18 (M2), and 12 days (MF) before starting the experiments. This preparation period enabled the initial densification of fresh snow through isothermal metamorphism [*Kaempfer and Schneebeli*, 2007; *Schleef and Löwe*, 2013], which resulted in a significant compaction of the initial height of the blocks (up to 8 cm for M2), hence a decreased SSA. The temperatures during the quasi-isothermal metamorphism were around -7°C, and temperature gradients never exceeded 5 K/m.

In M1 and M2, laboratory conditions were kept at 0°C during the entire duration of the experiments. The laboratory temperature during MF was set to oscillate between $+2$°C (heating, i.e., melting, periods) and -3°C (refreezing periods) to induce a much simplified process of the melt-freeze cycle, as often observed close to the snow surface. In all of the experiments, additional melt (hence water infiltration) was cyclically induced by placing a heating plate on top of the snow for $\sim$6–12 h/d, Figure 1d. Figure 2 reports the schedule of all the heating periods: this thermal input represents a similar process as occurring in a melting snow

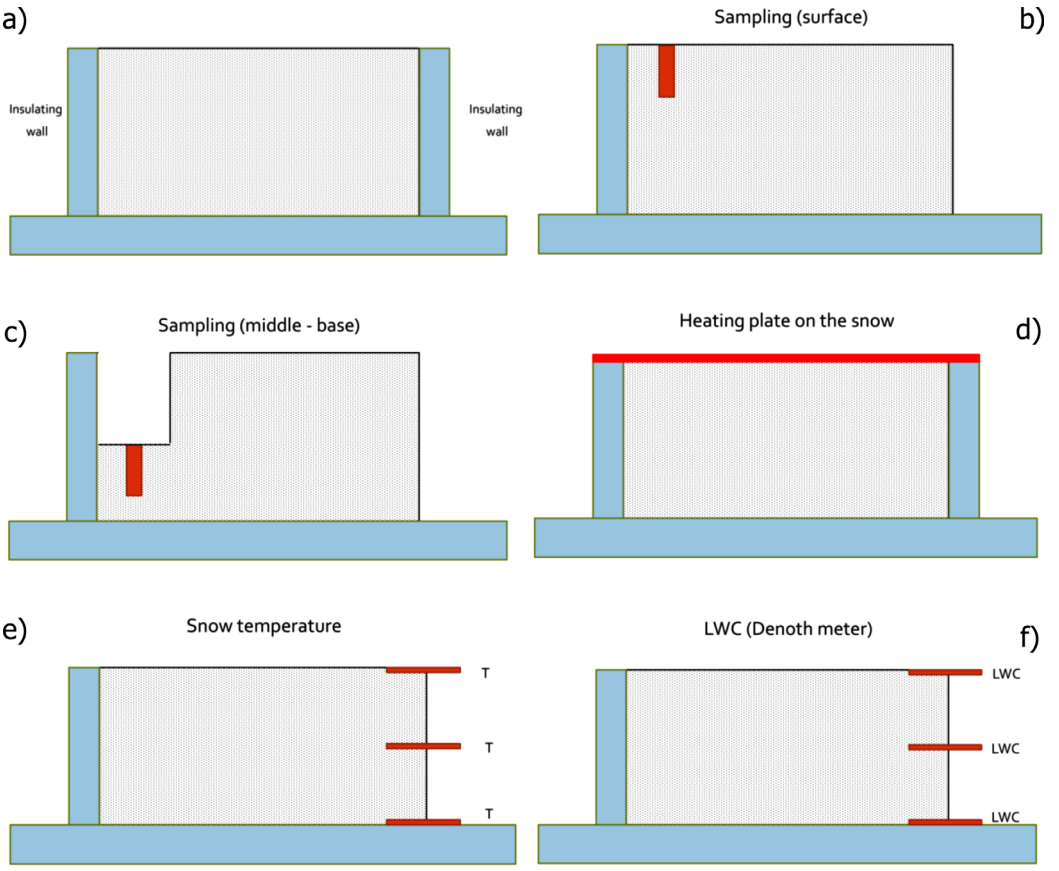

Figure 1. Sketch of the protocol defined to observe wet-snow metamorphism in the laboratory (Styrofoam walls are in blue): (a) snow block open to the environment; (b) probing surface samples with a cylindrical sample holder (in red); (c) probing middle and base samples with a cylindrical sample holder (in red); (d) heating plate (in red) over the surface of the snow; (e) measuring snow temperature at three different heights using manual temperature probes (in red); (f) measuring the LWC of the snow at three different heights using a Denoth meter (in red). Probing middle and base samples needed a portion of the block to be removed and then repositioned—Figure 1c.

cover during day-night cycles. We did not find a comparable protocol in the literature, especially for the MF experiment.

The heating plate used was rectangular in shape and had a finite defined resistance, which provided about 30 W/m^2. This power was not measured during the experiments as the resistance is constant and corresponds to a melt rate of 7.8 mm water equivalent/day. The use of a heating plate aimed at providing an additional energetic input and, therefore, at accelerating the melt process driven by ambient temperature. When placed on top of the snowpack, it covered most of the snow surface (about 5 cm of snow was not covered at two sides of the block). While the plate was in direct contact with the snow, no further compaction was observed. The plate created a homogeneous conductive forcing over the surface of the snow. At the end of each heating cycle, it was removed and the snow was exposed to the air.

Snow samples were periodically taken at different heights, Figures 1b and 1c. In the following, we refer to each sample using the name of the experiment and the label of the sample (for example, sample M1-A). Three reference positions were probed: snow surface, base, and middle, which refers to an average height with respect to the height of the block. Figure 2 reports the positions and labels of all the samples analyzed along with the temporal evolution of the height of the block. Available data are reported as blue dots, whereas the blue line represents an estimation obtained by assuming that the height of the block decreased with a constant rate during heating periods. The sample holders had a diameter of 28 or 37 mm and a height of 75 mm; we always report an estimation of the average height of sampling within the block.

The sample holders were directly pushed into the snow, and part of the snowpack was destructed by this process. In order to take samples at the base or in the middle of the block, a portion of the superficial snow

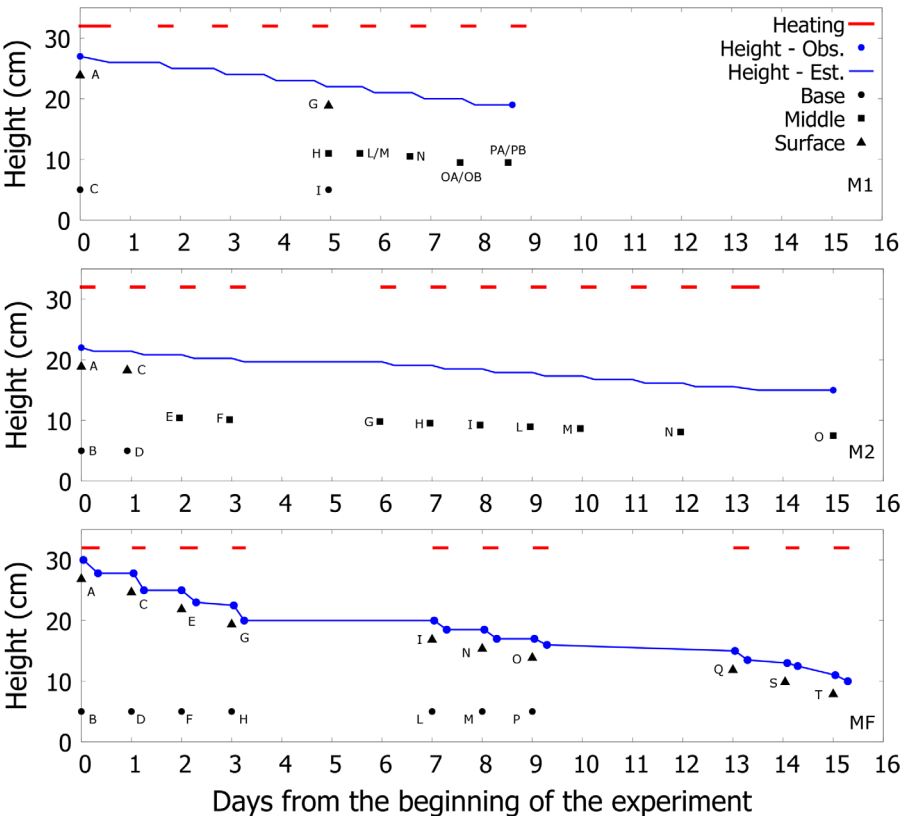

Figure 2. Timeline of the experiments: the red bars indicate heating periods, the blue dots and lines represent the measured and estimated height of the snow blocks. Symbols and letters indicate the position ("Surface," "Middle," and "Base") and the label of all the samples analyzed. In experiment M1, L and M are two different samples (vertical distance $\sim$ 3 cm); OA-OB and PA and PB are two different scans of the same sample (vertical distance $\sim$ 1.5 cm).

was manually removed, Figure 1c. Any further perturbation was avoided by re-positioning the removed snow after sampling; the following sampling area was then laterally moved. Even though basal runoff was allowed, a thick icy layer at the base of each block was created during the melt events due to capillary retention of liquid water [*Avanzi et al*., 2016]. This effect is also expected in the field at the interface between snow and soil, but represents a very specific condition that is not of interest for the study. Therefore, experiments M2 and MF were stopped when the height of the block reached approximately 15–10 cm. M1 was stopped after 8.5 days due to technical reasons.

Profiles of snow temperature were systematically performed during experiment MF to verify that the snow was at subfreezing conditions before starting a new heating period (i.e., refreezing was completed, Figure 1e). These measurements were taken performing periodic, manual measurements, and installing two iButton sensors at the base of the block and at 10 cm over the base (30 min temporal resolution). During the experiments, several measurements of the water content of the snowpack θ were also performed using a Denoth meter [*Denoth*, 1994], Figure 1f. These measurements were not periodic, as the snowpack was too small in size for these semidestructive measurements.

2.2. Microstructural Measurements and Calculations

Each sample was scanned using X-ray microcomputed tomography (micro-CT SCANCO μ40). During M1 and M2, samples were taken in wet snow and immediately stored at subfreezing conditions in order to freeze the liquid water. During the MF experiment, refrozen snow samples were always extracted before starting a new melt cycle. While some promising results for other multiphase systems have been recently reported in the literature [*Obbard et al*., 2009; *Pinzer et al*., 2012; *Obbard*, 2015], the segmentation of all three phases (ice, liquid, and air) has indeed proved very difficult for the dimensionally small ice microstructure and local, thin intrusions of water considered in the experiments (see section 3). As the liquid water content

was below about 5% water per volume (see section 4), the retrieval of the structural parameters is affected systematically, but cannot be quantified with current methods.

The nominal(effective) resolution chosen was 18(30) μm for the experiments M1 and M2 and 30(35) μm during MF. To reduce image noise, the raw sinogram of the micro-CT was measured by averaging two images with an integration time of 300 ms, reconstructed, filtered with a 3^3 Gaussian filter and visually segmented into ice and air [*Hagenmuller et al.*, 2016]. The segmentation of the images was done by visually selecting the valley between the histogram peaks; the thresholds were not constant, but varied by about 3%, which does not change density and SSA by more than 3%. The evaluated volume (region of interest) was at least 1028 × 1028 × 410 voxels (length × width × height, experiments M1 and M2) and 516 × 516 × 305 voxels (length × width × height, experiment MF), or 18.5 × 18.5 × 7.4 mm (length × width × height, experiments M1 and M2) and 15.5 × 15.5 × 9.15 mm (length × width × height, experiment MF). This volume is larger than the homogeneous, representative elementary volume (REV) needed to compute permeability [*Zermatten et al.*, 2011; *Calonne et al.*, 2012], which is a key parameter ruling unsaturated water flow and may be therefore a good benchmark for structural computations in wet snow. An increase in size of the processed voxel reduces the noise and returns a better signal to noise; the change did not affect any calculation.

The structural parameters: density, SSA, and ice structure and pore thickness distribution were all calculated by using the Image Processing Language IPL [*Hildebrand and Rüegsegger*, 1997; *Kaempfer and Schneebeli*, 2007]. SSA was calculated as the ratio between ice surface and ice mass (m^2/kg) [*Fierz et al.*, 2009]. The ice and pore thickness distribution for each sample was obtained by approximating the ice and pore matrix, respectively, with a collection of maximal spheres, the diameters of which represent the local thickness [*Hildebrand and Rüegsegger*, 1997; *Löwe et al.*, 2011]. Thickness thereby is a measure of grain size. While absolute SSA is within 10% error [*Hagenmuller et al.*, 2016], changes in SSA have much less uncertainty, as we used always the same procedure for filtering and segmenting the images.

3. Results

Figures 3–5 report the micro-CT 3-D reconstructions of some samples taken during the three experiments. Figures 6–8 report the temporal evolution of SSA, statistical moments, and thickness distributions for the three experiments. The supporting information includes for each sample: a 3-D reconstruction, a map of ice thickness within one vertical section, and frequency density and cumulative distribution of ice thickness (supporting information Figures S1–S41). Measurements of liquid water content and snow/air temperature during experiment MF are also reported (supporting information Figures S42 and S43).

3.1. Three-Dimensional Reconstruction

Figures 3–5 show that the initial conditions of all the experiments were homogeneous (M1-A, M2-A, and MF-A). With time, structural evolution in wet conditions led to progressive coarsening. Grain growth was very variable in space, that is, the ice matrix evolved from homogeneous conditions to heterogeneous clustering of coarse grains (see e.g., samples M1-I, M1-M, M1-N, M2-F, M2-H, MF-G, and MF-Q). The increase in size of grains outside the clusters was much slower (see sample M1-M, M1-N, or M2-F). Samples M2-N or M2-O reveal that continuous melting led to a prevalence of coarse structures in M2, i.e., a spatially more homogeneous condition than intermediate samples. In MF, structural evolution was slower (see e.g., sample MF-T).

3.2. SSA and Density

SSA decreases from initial (SSA ∼ 19–28 m^2/kg) to final samples (SSA ∼ 18–13 m^2/kg in M1, ∼5 m^2/kg in M2, and ∼8–13 m^2/kg in MF), see Figures 6a, 7a, and 8a. In M1 and M2, the variability between simultaneous or consecutive measurements is rather large. In MF, the variability between observations increases with time. The coefficient of determination (r^2) of a linear regression of SSA versus time (in days) for samples taken at middle height in M2 reads $r^2 = 0.60$. In MF, $r^2 = 0.89$ and 0.83 when considering samples taken at surface and at the base, respectively. In M1, the slope (m), y-intercept (q), and r^2 for samples taken at middle height read (95% confidence bounds in brackets): $m = 0.18$ $m^2/kg/d$ (–2.41 to 2.78 $m^2/kg/d$), $q = 13.08$ m^2/kg (–5.07 to 31.22 m^2/kg), and $r^2 = 0.005$. Because the confidence bounds for m include zero, this

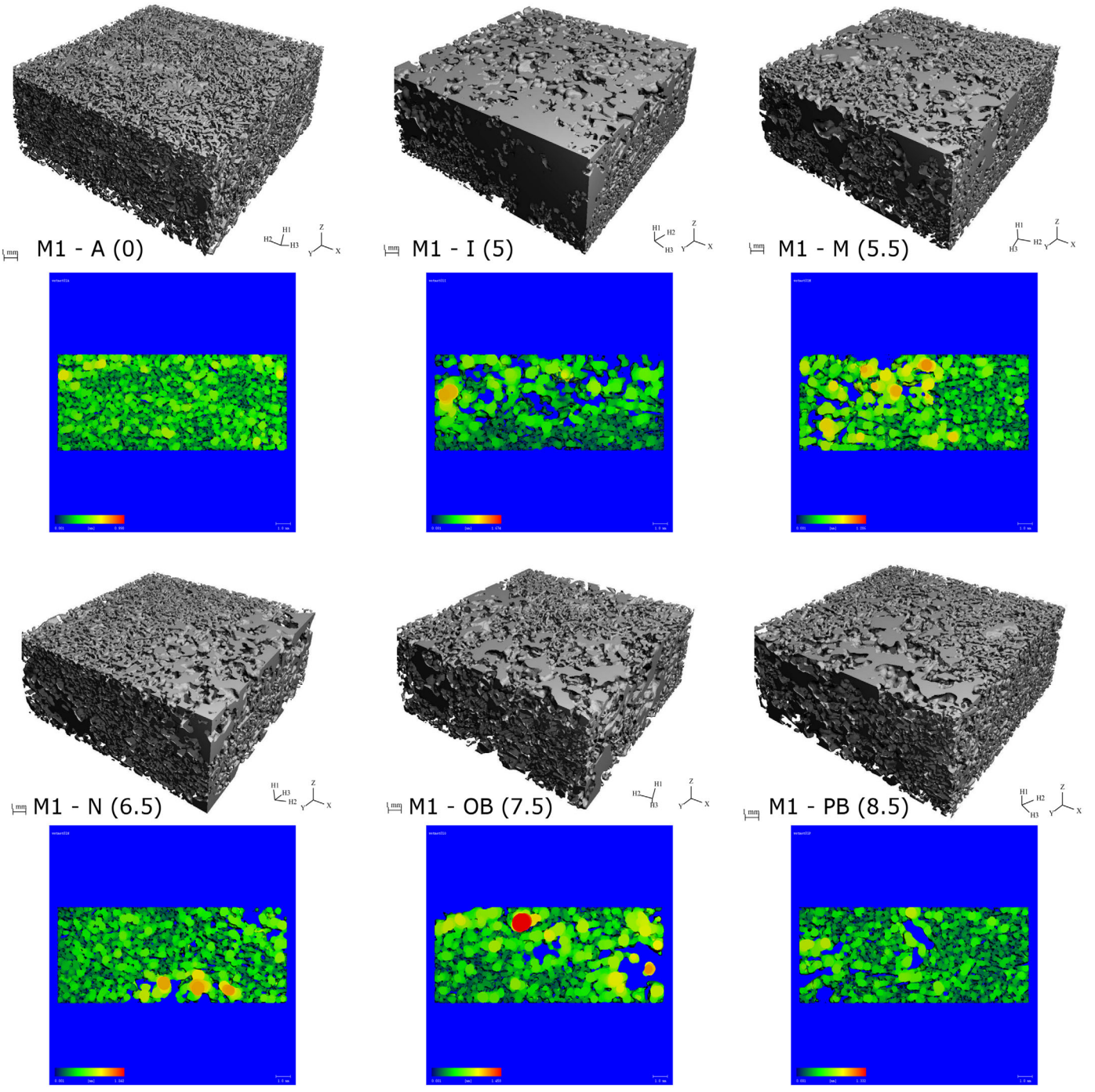

Figure 3. Three-dimensional reconstruction and one vertical section of some samples taken during experiment M1. The color scale of the section represents the size of maximal spheres (see section 2.2). Larger versions of all the figures and of scale bars are reported in the supporting information for the sake of readability.

increase with time is not significant [*Kottegoda and Rosso*, 2008], probably because of the short duration of this experiment (~200 h). The decrease in SSA for M2 and MF is significant at 95%.

Initial density was equal to about 210 kg/m^3 (M1-A/M1-C), 240 kg/m^3 (M2-A/M2-B), and 216 kg/m^3 (MF-A/MF-B). It increased up to approximately 450 kg/m^3 (M2-M, after 10 days) or up to approximately 300–400 kg/m^3 (MF-Q, MF-S, and MF-T, after 13–15 days); this is due to both settling and pore saturation with water.

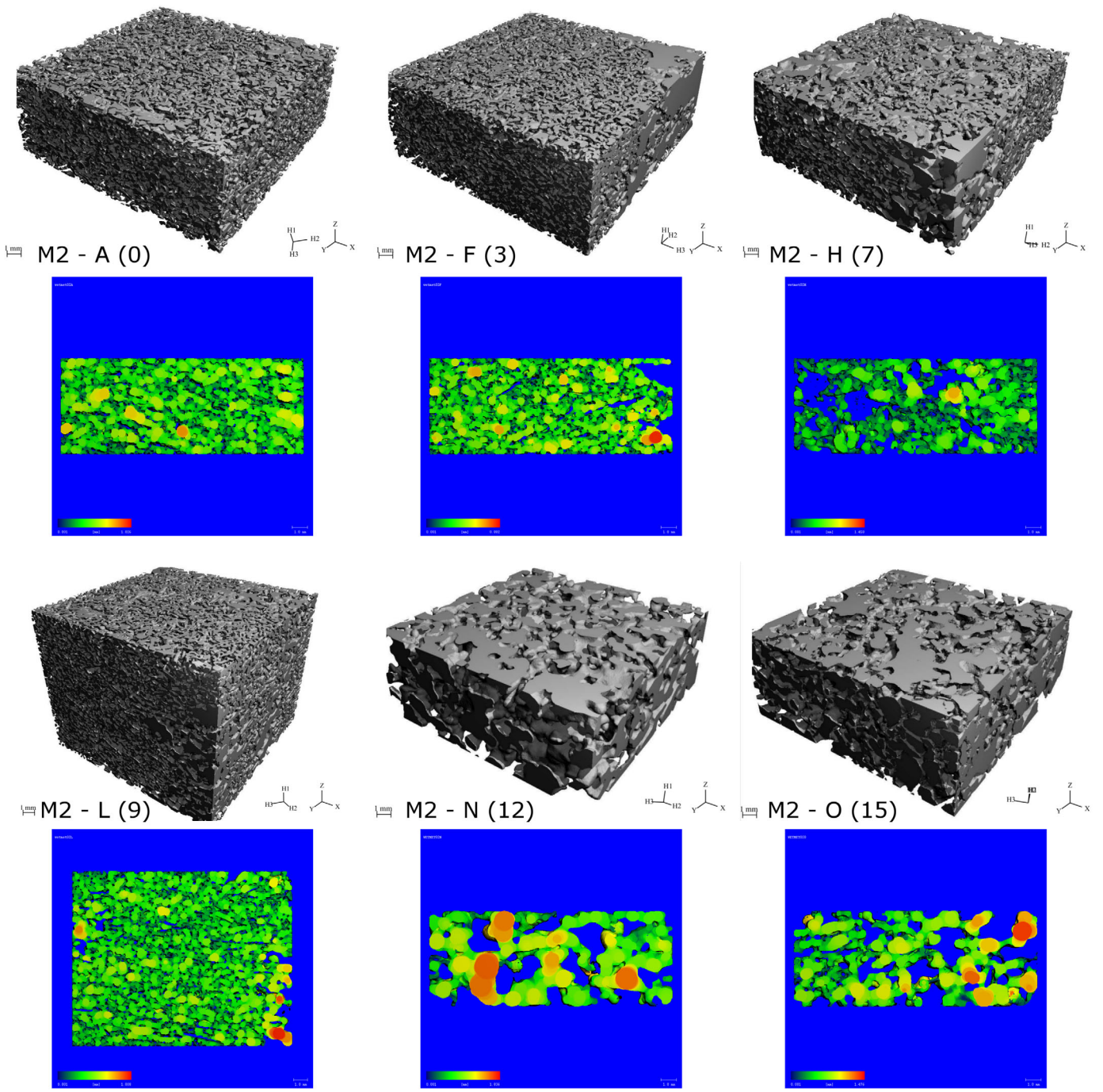

Figure 4. Three-dimensional reconstruction and one vertical section of some samples taken during experiment M2. The color scale of the section represents the size of maximal spheres (see section 2.2). Larger versions of all the figures and of scale bars are reported in the supporting information for the sake of readability.

3.3. Thickness Distribution

The mean of structure thickness (μ, mm, see Figures 6b, 7b, and 8b) and its standard deviation (σ, mm, see Figures 6c, 7c, and 8c) tend to increase with time in the experiments. In M1, a linear regression of μ versus time yields $r^2 = 0.22$, but the 95% confidence bounds of the slope include zero (–0.01 to 0.06 mm/d), thus this increase is not significant. The increase in σ is significant at 95% (m between 0.002 and 0.06 mm/d). The coefficient of variation $CV = \sigma/\mu$ also returns a significant increase with time (m between 0.05/day and 0.11/day, 95% confidence bounds). In M2, the increase in mean thickness is significant ($r^2 = 0.70$, m between

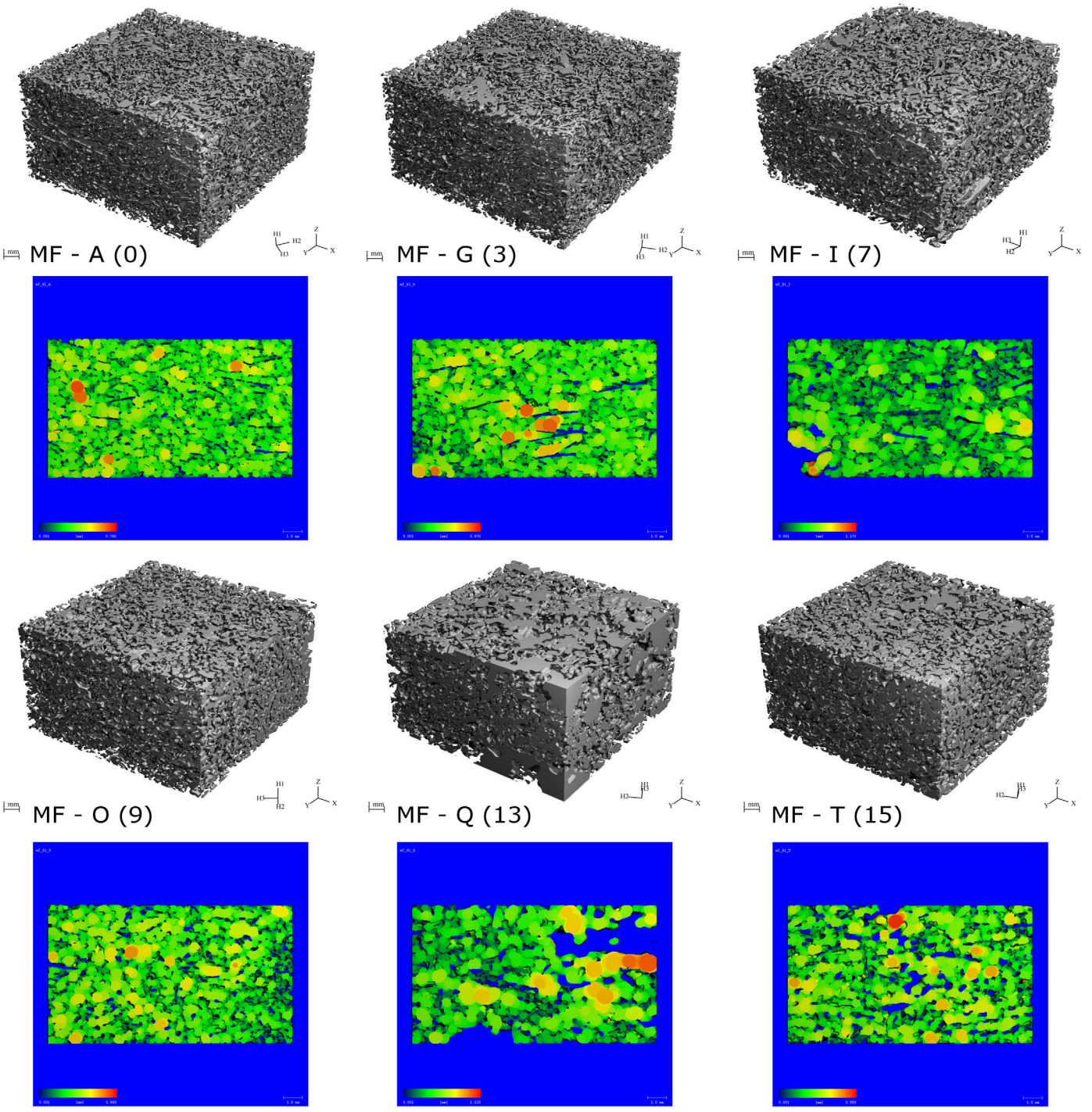

Figure 5. Three-dimensional reconstruction and one vertical section of some samples taken during experiment MF. The color scale of the section represents the size of maximal spheres (see section 2.2). Larger versions of all the figures and of scale bars are reported in the supporting information for the sake of readability.

0.03 and 0.07 mm/d, 95%), but the variability between consecutive (or simultaneous) samples is large. For example, μ varies among 0.19, 0.52, and 0.34 mm between days 2 and 6. The increase in σ is significant as well (m between 0.002 and 0.04 mm/d), whereas the CV shows no significant trend (both at 95%). The increase in μ ($r^2 = 0.56$) and σ in experiment MF is slower but significant; the increase of CV with time is also significant (all at 95%). For this experiment, the variability between consecutive measurements increases with time (see e.g., samples MF-Q, MF-S, and MF-T).

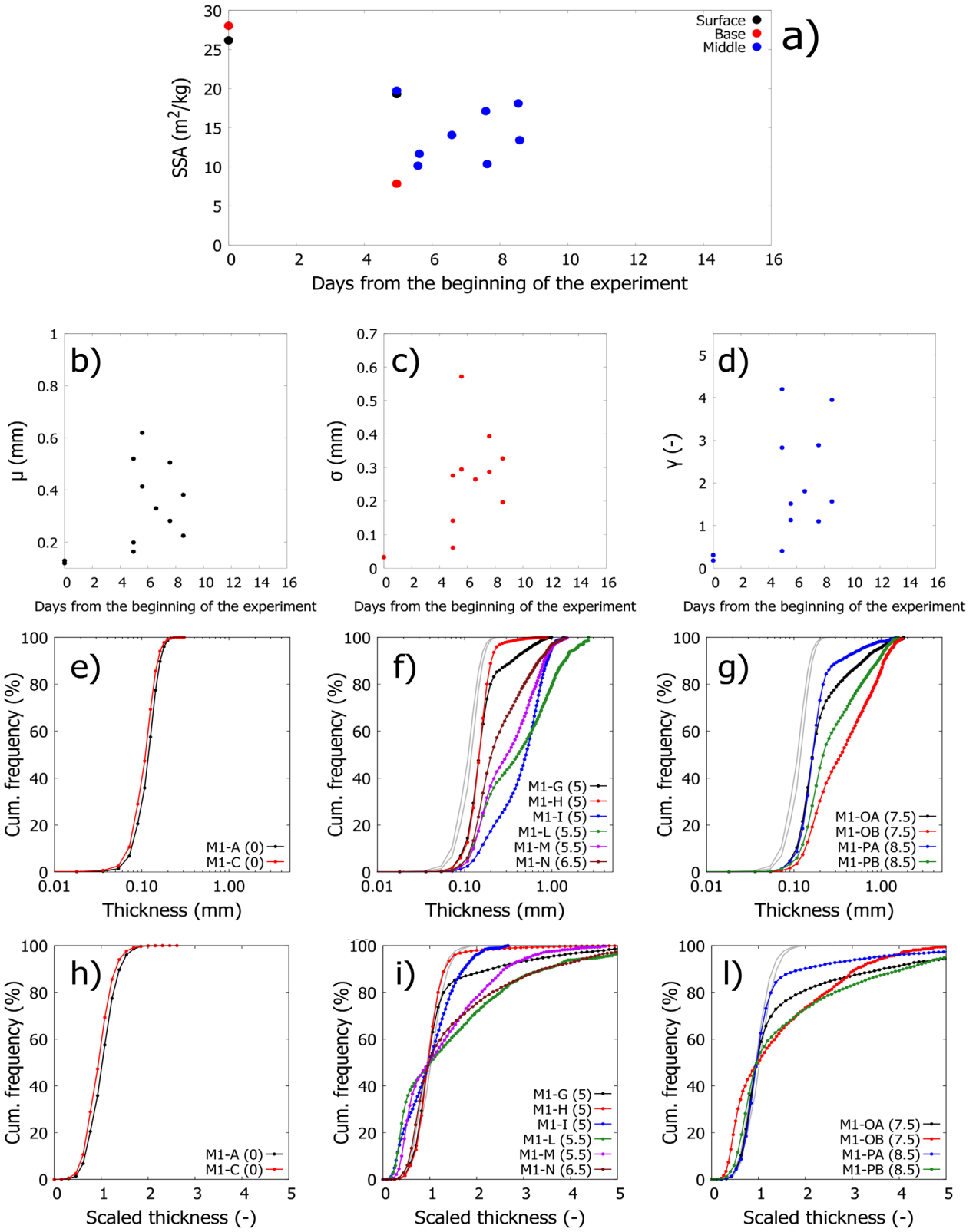

Figure 6. Statistics of experiment M1: (a) SSA; (b–d) mean (μ, mm), standard deviation (σ, mm), and skewness (γ, -) of thickness distributions; (e–g) thickness distributions; (h–l) scaled thickness distributions. Grey lines in Figures 6f, 6g, and 6i–6l refer to samples M1-A and M1-C and are reported for reference.

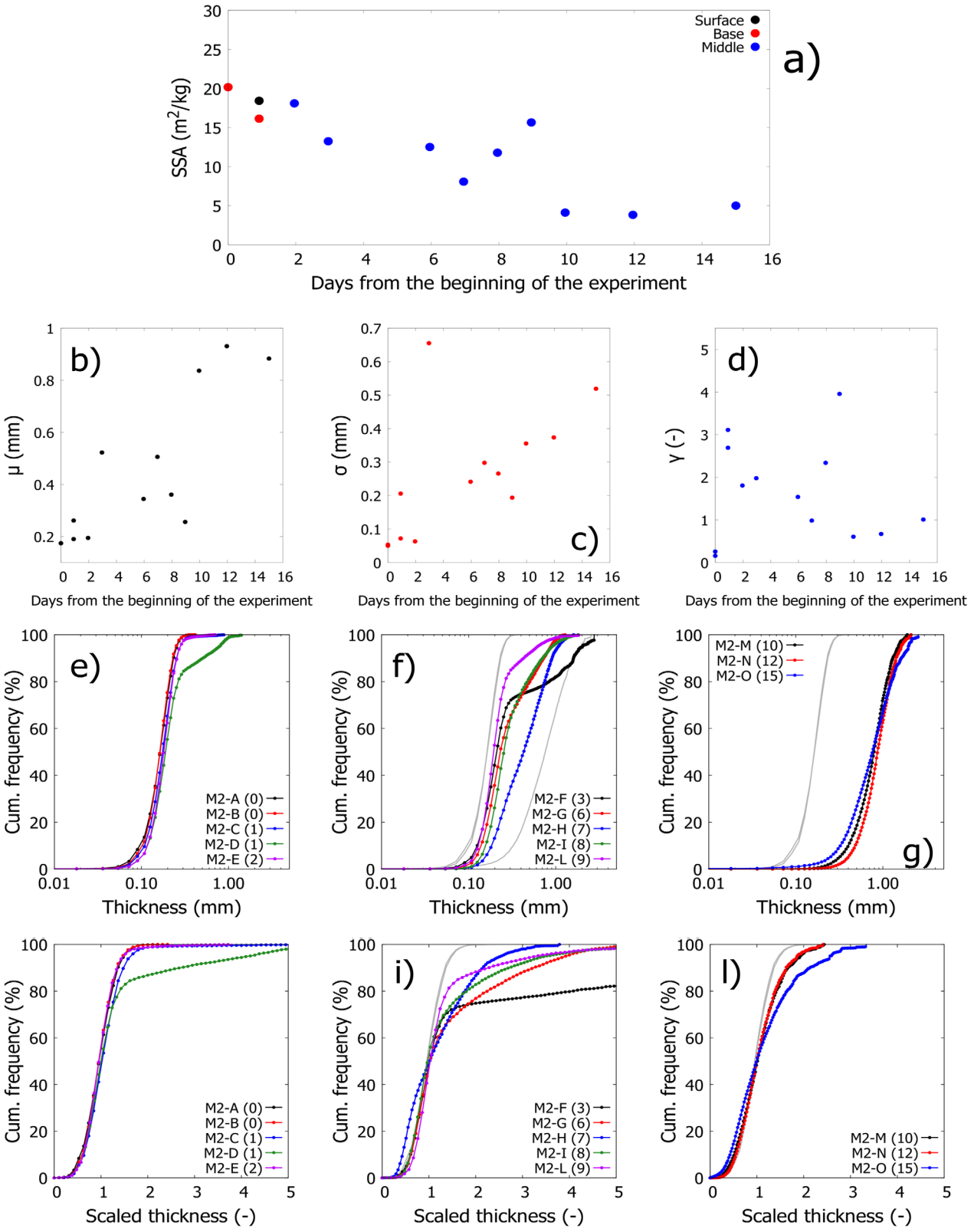

Figure 7. Statistics of experiment M2: (a) SSA; (b–d): mean (μ, mm), standard deviation (σ, mm), and skewness (γ, -) of thickness distributions; (e–g) thickness distributions; (h–l) scaled thickness distributions. Grey lines in Figures 7g and 7i–7l refer to samples M2-A and M2-B and are reported for reference. In Figure 7f, grey lines refer to M2-A, M2-B (left), and M2-O (right).

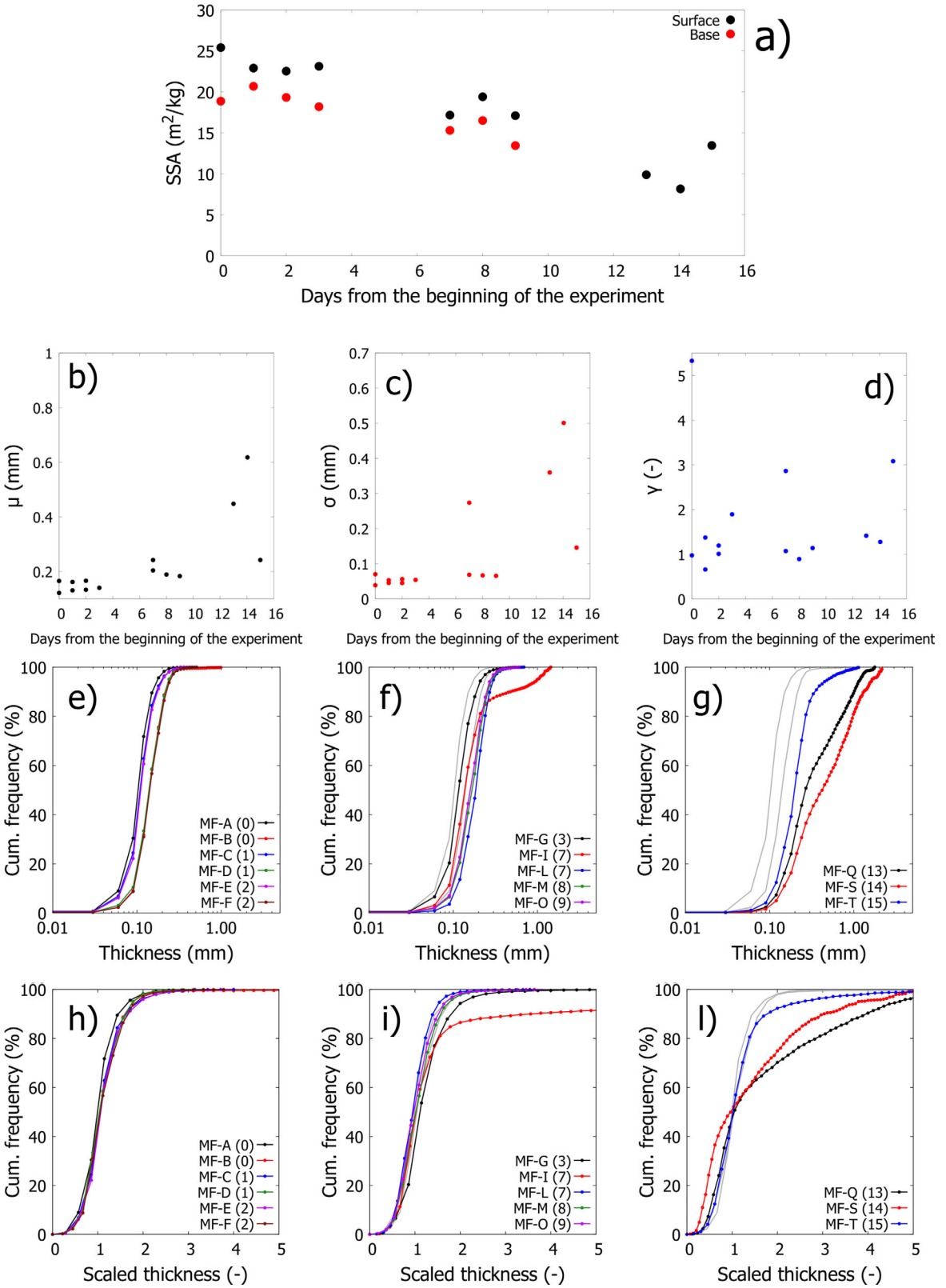

Figure 8. Statistics of experiment MF: (a) SSA; (b–d) mean (μ, mm), standard deviation (σ, mm), and skewness (γ, -) of thickness distributions; (e–g) thickness distributions; (h–l) scaled thickness distributions. Grey lines in Figures 8f, 8g, and 8i–8l refer to samples MF-A and MF-B and are reported for reference.

Skewness (γ, -) is initially quite small, i.e., ≤ 1 in 5 out of 6 samples (Figures 6d, 7d, and 8d). Sample MF-B shows a very high γ, which is probably due to local heterogeneity in snow structure created during sieving. Its mean and standard deviation are, however, consistent with other initial samples. A linear regression of skewness versus time returns no significant slope for any experiment and a small coefficient of determination ($r^2 = 0.28$ in M1, 0.006 in M2, and 0.0005 in MF, 95%), which is consistent with the observed large variability between consecutive samples.

Cumulative frequency distributions (Figures 6e–6g, 7e–7g, and 8e–8g) shift toward a higher thickness with time; they also widen their range and increase in mode (see the supporting information for frequency density distributions). During early coarsening, the right tail of the distribution becomes heavier and longer, while the shift of the central part of the distribution and of its left tail is reduced (see e.g., M1-G, M1-H, M2-F, M2-L, MF-I, and MF-T). At a later stage, the central part of the distribution and the left tail shift, while the position of the right tail is fixed. In M2, this second stage approximately starts after 7–10 days, sample M2-H and M2-M. Other examples are M1-OB or MF-S.

Samples taken at consecutive measurement times show a marked variability in the thickness distribution. For example, M1-L and M1-M are two samples taken on the same day at a vertical distance of $\sim$3 cm; OA-OB and PA-PB were sampled at a vertical distance of $\sim$1.5 cm. While M1-L and M1-M differ for percentiles higher than $\sim$40% (thickness $>$ 0.15 mm), OB and PB present a higher thickness for all percentiles and a lower peak for the mode than OA and PA (see also supporting information Figures S9–S12). Both features indicate a much coarser structure in these samples than in OA and PA, despite their small distance.

Following *Raymond and Tusima* [1979], we scale now the thickness distribution of each sample in units of a characteristic size (median thickness). *Raymond and Tusima* [1979] measured particle size using optical microscopy, thus they suggest to plot the distributions in units of the median diameter or the median volume of particles. Because structural evolution during wet-snow metamorphism leads to fast rounding of particles, this characteristic is comparable to the available thickness distributions obtained using maximal spheres (Figures 6h–6l, 7h–7l, and 8h–8l). Scaled distributions generally overlap up to a percentile equal to 60%–80%. For higher percentiles, initial samples (e.g., M1-A and M1-C, M2-A and M2-B, or MF-A and MF-B) show small differences, while following samples show much larger differences and nonoverlapping, heavier and longer right tails. In M2, this shift recedes in final samples: the scaled distributions of M2-M, M2-N, and M2-O are closer to initial conditions than to intermediate samples. In all the experiments, some samples show discrepancies even for small percentiles; examples are M1-I, M2-H, and MF-S. Dynamics during melt-freeze are generally slower than during continuous melting.

We test the hypothesis of same thickness distribution for subsequent samples belonging to the same experiment using a two-sample Kolmogorov-Smirnov test (KS2) [*Kottegoda and Rosso*, 2008]. Because available thickness distributions are discrete and contain ties (i.e., repeated values due to resolution effects), we performed the test using a Monte-Carlo technique and extracting 2000 synthetic distributions from each sample, which were then compared one by one (see supporting information Figure S44). The cardinality of these synthetic distributions is set to 250 following *Colbeck* [1986a]. For each couple of samples, the test is assumed rejected if the p value of the KS2 is smaller than the significance level (0.05) in either 50% or 90% of the couples of synthetic distributions. While the test is rejected for 37% (64%) of the couples of samples in MF setting the threshold to 90% (50%), it is rejected for 74% (91%) of the cases in M1 and 56% (83%)of the cases in M2 (again setting the threshold to 90% or 50%, respectively). Overall, this test rejects the (null) hypothesis of same distribution in 78% of the couples of samples (threshold to 50%). The test is rejected for 54% of the couples if the threshold is set to 90%. This statistical analysis indicates that the thickness distribution was not time-invariant in these experiments.

4. Discussion

4.1. The Role of Heterogeneity

These results reveal fast coarsening during continuous melting or melt-freeze, in agreement with the previous works by *Wakahama* [1968], *Colbeck* [1973], *Raymond and Tusima* [1979], *Colbeck* [1986a], and *Brun* [1989]. *Marsh* [1987] also observed a widening of the grain size range during wet-snow metamorphism in the field. However, data suggest that grain growth during wet-snow metamorphism in our experiments was marked by large spatial heterogeneity, even if the initial properties of the snowpack as well as external

heating were spatially very homogeneous. Previous experiments about wet-snow metamorphism in the laboratory did not report such a large heterogeneity of coarsening, probably because they used soaked particles [*Raymond and Tusima*, 1979] or homogeneously electromagnetically heated samples [*Brun*, 1989]. Both choices promote homogeneity of wet-snow metamorphism, but, in most cases, represent idealized conditions compared with natural wetness, which is marked by complex, heterogeneous patterns during infiltration [*Waldner et al*., 2004; *Techel and Pielmeier*, 2011; *Avanzi et al*., 2016]. The temporal evolution of thickness distributions and the visual inspection of 3-D images suggest that the observed heterogeneity originated at mm scale (i.e., at subsample scale). At a larger scale, the observed structural heterogeneity caused large variability in SSA as well as several nonsignificant trends in statistical moments (see Figures 6–8).

Measurements of liquid water content during our experiments show peaks around 3–4 vol %, i.e., a very low liquid saturation (see supporting information Figure S42). Available observations of snow temperature during MF also show that the snow blocks were in isothermal conditions at 0°C during heating periods (see supporting information Figure S43). While clusters of single, rounded grains can develop at low saturation [*Colbeck*, 1979, 1986b], the available scans show that in these experiments such clusters coexisted with much finer snow grains (see e.g., M1-PB or M2-H). The initial structure of snow and the external forcings were all spatially homogeneous; thus, it is unlikely that this outcome was caused by the experimental geometry. Also, the preparation period (see section 2) limited the overlap between the observed coarsening and the initial changes in grain structure and morphology of fresh snow [*Kaempfer and Schneebeli*, 2007]. Because wet-snow metamorphism is mainly driven by local liquid water content [*Brun*, 1989], such a high spatial heterogeneity in coarsening could be explained by spatial heterogeneity in wetness. Preferential infiltration of liquid water in snow has been observed both in the field [*Marsh and Woo*, 1984b, 1985; *Schneebeli*, 1995] and in the laboratory [*Waldner et al*., 2004; *Avanzi et al*., 2016]. Recently, *Katsushima et al*. [2013] found that preferential flow may occur even in vertically homogeneous, isothermal snow. The onset of preferential flow concentrates water in highly saturated channels [*Waldner et al*., 2004]. As a result, grain growth is locally enhanced by the presence of a local, larger liquid water content.

4.2. Homogeneous Versus Heterogeneous Grain Growth

Preferential flow plays an important role in ruling liquid water in snow [*Schneebeli*, 1995], but exhaustive observations of snow structural evolution during heterogeneous percolation are still missing. Our results suggest that heterogeneous infiltration of water and wet-snow metamorphism were in our experiments intrinsically coupled at grain scale, i.e., the heterogeneous percolation of water into initially homogeneous snow quickly led to local, preferential coarsening. In terms of thickness distribution, preferential coarsening thickens the right tail. Because coarsening is localized in areas affected by preferential infiltration, thickness slowly increases in other areas of the snowpack. A limit case is sample M1-I, which suggests a bimodal distribution of grain growth (see supporting information Figure S5). A feedback between infiltration of liquid water and local coarsening may also explain the discrepancy between scaled thickness distributions for different times, which contrasts with previous observations by *Raymond and Tusima* [1979] and *Colbeck* [1986a], who observed shape invariance of particle size distributions in saturated snow and invariance of scaled thickness distributions with time [*Colbeck*, 1986a].

Samples M2-M, M2-N, and M2-O show that continuous melting may lead to the homogenization of snow structure. Scaled distributions for these samples show, indeed, an increased overlap with initial distributions, Figure 7l. This property is very similar to previous observations by, e.g., *Wakahama* [1968], *Raymond and Tusima* [1979], and *Colbeck* [1986a]. Thus, wet-snow metamorphism in our experiments suggests two strikingly different structural sizes: homogeneous coarsening superimposed by faster heterogeneous coarsening in areas affected by preferential infiltration of water. While there is always a coarsening when snow is at 0°C, this heterogeneity suggests enhanced wet-snow metamorphism in areas of preferential channels.

Schneebeli [1995] observed that the location of preferential channels in snow is not stable in space and time. Because areas affected by preferential infiltration may change with time due to instability of fingers, heterogeneous, early coarsening may progressively lead to a more homogeneous structure. Spatial migration of preferential paths may be related with external forcings [*Schneebeli*, 1995], as the chosen heating scheme was intermittent in time. It may also present a strong coupling with coarsening, as grain growth modifies the hydraulic properties of snow, e.g., permeability [*Calonne et al*., 2012] and the water retention curve [*Yamaguchi et al*., 2010, 2012]. Because of the relatively small size of samples, these results cannot be

upscaled to include, e.g., structural evolution of snow in macropores [*Kattelmann*, 1985]. This size is, however, consistent with the expected process scale [*Blöschl*, 1999] of preferential flow. While its physical basis is not clear yet [*Schneebeli*, 1995; *Katsushima et al*., 2013], this seems, indeed, related with local instability of the wetting front at grain scale [*Katsushima et al*., 2013; *Hirashima et al*., 2014; *Baver et al*., 2014]. Imaging the full extent of these fingers is not possible by the current setup of the micro-CT. An unbiased statistical analysis of preferential wet-snow metamorphism is therefore not possible (see section 4.4).

While the distance between middle samples and the heating plate slightly decreased during experiments M1 and M2 (see Figure 2), the emergence of a heavier right tail and of clusters of large grains were also observed during experiment MF, which included only basal and superficial samples. A comparison between melting and melt-freeze experiments reveals that the rate of wet-snow metamorphism at low saturation decreased during repeated melt-freeze cycles. This is likely due to the shorter duration of wet periods in experiment MF. Furthermore, cyclic liquid water infiltration in MF occurred in initially subfreezing snow. Refreezing of water in cold snow can sensibly delay the advance of the wetting front or of preferential fingers [*Marsh and Woo*, 1984b]. Consequently, areas affected by wet-snow metamorphism as well as by fingers may be spatially very localized; this may explain the smaller variability between consecutive measurements of SSA. The increases in variability with time is likely due to enhanced grain growth in areas affected by preferential infiltration and melt-freeze [*Marsh*, 1987].

4.3. Implications

These observations have important implications for snow modeling. First, they challenge existing parametrizations of wet-snow metamorphism, which have been formulated using results in homogeneous, wet conditions. Experiments show, indeed, a dramatic increase in both spatial heterogeneity at local scale and large temporal variability in the evolution of bulk properties, such as SSA or mean thickness. The formation of preferential flow at an early stage, and the consequently spatially heterogeneous coarsening, make the definition of a unique REV difficult. The definition of representative conditions for parametrization in wet snow, therefore, remains an open issue. As the unsaturated permeability is not only a parameter defined by its geometry (as for saturated flow), but also by the water content, the concept of an REV is, for example, difficult, if not impossible to apply for this parameter (see section 2.2). Our measurements remain therefore to a certain degree descriptive, and cannot be statistically quantified.

Second, our experiments show that the formation of preferential flow paths directly affected coarsening. Tracer experiments have shown this for a long time, but were not interpreted with respect to coarsening at an early stage. Because snow structure is nonlinearly related with water flow through retention properties and hydraulic conductivity, locally enhanced coarsening may represent an important, but still poorly investigated, process in driving unsaturated infiltration in snow and fast initialization of preferential flow. This coupling may be included in existing multidomain [*Wever et al*., 2016b] or multidimensional [*Hirashima et al*., 2014] models by altering the description of hydraulic properties in preferential channels compared to that in homogeneous conditions [*Wever et al*., 2016b].

Third, the observed evolution of wet-snow metamorphism does not show shape invariance of thickness distribution, contrary to previous observations. This result suggests that the initial preferential infiltration of water in snow causes a transient behavior of wet-snow metamorphism compared with spatially homogeneous conditions. Future experiments and models should take into account this observation.

4.4. Experimental Limitations and Outlook

While we cannot imagine a different process that leads to the observed coarsening than liquid water, an important limitation of these experiments is the lack of direct observations and/or measurements of LWC. This is due to the small size of the samples, which hampers the use of existing instrumentation as there is currently no technique to measure the heterogenous distribution of water content in snow at the scale observed (see *Kinar and Pomeroy* [2015], for a review). Additional insight into the dynamics of wet-snow metamorphism in natural-like conditions may be obtained by coupling X-ray microtomography with detailed observations of liquid water flow at pore scale [*Walter et al*., 2013] or multiphase segmentation of micro-CT data [*Pinzer et al*., 2012]. While experiment MF was explicitly designed to include melt-freeze cycles, available observations of LWC suggest that the volume occupied by liquid water during M1 and M2, hence its relevance for structural computations, should be small. For example, refreezing the liquid water

does not lead to a substantial change in density, as LWC is always below 5% volume. This conclusion is also supported by the overall agreement between M1-M2 data and MF data of structural evolution in melting snow. Liquid water in snow at low saturation is, however, held in capillary menisci [*Colbeck*, 1980], which can locally increase the LWC and speed-up grain growth even though water occupies only a thin film. Also, refrozen menisci may represent an important source of uncertainty in thickness computation. The complex geometry of these films makes it impossible to simply quantify the expected bias. Detecting the three phases of wet snow could, thus, assist in quantifying the uncertainty introduced by refreezing snow samples before scanning.

While heterogeneous grain growth was observed during all the experiments, the transition to homogeneous grain growth was fully observed only during M2. A longer duration and a larger amount of experiments could be useful to generalize these observations and, therefore, to include natural-like conditions in existing parametrizations. Because natural snow in field conditions is subjected to a variety of thermal, hydraulic, and mechanical processes, future work should also consider different initial properties of snow (e.g., density) and different energy inputs. This includes the use of infrared lamps for inducing snowmelt [*Waldner et al*., 2004], which could avoid any direct interaction with the snowpack but would also complicate the boundary condition. Also, different sampling protocols and a larger amount of samples could be useful for better characterizing the variability of wet-snow metamorphism at the snowpack scale.

While this work represents a first step toward understanding natural-like wet-snow metamorphism, it also shows that carrying out wet-snow experiments representative of field conditions is challenging because measurements can perturb the ongoing phase change. Also, snowmelt decreases the height of the block and introduces edge effects at its boundary, which progressively reduces the available space for sampling. As mentioned, the development of preferential flow patterns may need a larger snow volume than that currently used for micro-CT structural computations [*Katsushima et al*., 2013; *Avanzi et al*., 2016]. Past experimental measurements show indeed that typically the spacing between preferential flow paths is in the range from several centimeters to decimeters [*Marsh and Woo*, 1984b; *McGurk and Marsh*, 1995; *Williams et al*., 2010]. A necessary volume would be at least several liters, and would require a scan diameter of several decimeters. This hampers the use of forced temperature cycles within a sample chamber like in *Pinzer et al*. [2012]. Further efforts are needed to develop a full description of 3-D dynamics of wet-snow metamorphism starting from the existing theory in homogeneous conditions, the observed spatial heterogeneity, and improved experimental techniques.

5. Conclusions

We observed wet-snow metamorphism using X-ray microtomography during continuous vertical infiltration of water due to melting, or melt-freeze. This protocol is significantly different from previous experiments focused on soaked snow or initially homogeneously unsaturated snow. Experiments suggest that wet-snow metamorphism is marked by high spatial and temporal variability due to fast initialization of preferential flow in an initially homogeneous snowpack. The specific surface area of the ice matrix decreased with time and the mean thickness, a measure of grain size, increased, even though these dynamics are significant only for longer experiments (M2 and MF). Both results are in agreement with existing literature, but they also show high variability between consecutive observations. Thickness distributions suggest that, in these experiments, wet-snow metamorphism showed two different patterns due to early formation of preferential flow at local scale and coupled structural evolution: homogeneous coarsening was superimposed by localized grain growth in areas affected by preferential infiltration of water. Thus, thickness distributions did not show shape invariance with time. The dynamics of wet-snow metamorphism slowed during melt-freeze. The transition from highly heterogeneous coarsening to homogeneous grain growth may be explained by instability of preferential flow paths with time. Additional experiments are highly needed to confirm the observed spatial variability of wet-snow metamorphism and to include it in existing parametrizations.

Acknowledgments
The laboratory assistance and micro-CT measurements by Matthias Jaggi and Amy Macfarlane are gratefully acknowledged. Author contributions: M.S., G.P., and F.A. designed the experiments. G.P. and F.A. analyzed the data, all authors contributed to the writing of the manuscript. Data are available at https://doi.org/10.1594/PANGAEA.874393. We thank Günter *Blöschl*, Editor, Nick Rutter, Associate Editor, and two anonymous reviewers for providing insightful comments on the manuscript.

References

Avanzi, F., H. Hirashima, S. Yamaguchi, T. Katsushima, and C. De Michele (2016), Observations of capillary barriers and preferential flow in layered snow during cold laboratory experiments, *Cryosphere*, *10*(5), 2013–2026, doi:10.5194/tc-10-2013-2016.

Bartelt, P., and M. Lehning (2002), A physical SNOWPACK model for the Swiss avalanche warning Part I: Numerical model, *Cold Reg. Sci. Technol.*, *35*, 123–145, doi:10.1016/S0165-232X(02)00074-5.

Baver, C. E., J. Y. Parlange, C. R. Stoof, D. A. DiCarlo, R. Wallach, D. S. Durnford, and T. S. Steenhuis (2014), Capillary pressure overshoot for unstable wetting fronts is explained by Hoffman's velocity-dependent contact-angle relationship, *Water Resour. Res.*, *50*, 5290–5297, doi:10.1002/2013WR014766.

Blöschl, G. (1999), Scaling issues in snow hydrology, *Hydrol. Processes*, *13*(14-15), 2149–2175, doi:10.1002/(SICI)1099-1085(199910)13:14/15 < 2149::AID-HYP847 > 3.0.CO;2-8.

Brun, E. (1989), Investigation on wet-snow metamorphism in respect of liquid-water content, *Ann. Glaciol.*, *13*, 22–26.

Brun, E., P. David, M. Sudul, and G. Brunot (1992), A numerical model to simulate snow-cover stratigraphy for operational avalanche forecasting, *J. Glaciol.*, *38*(128), 13–22, doi:10.3198/1992JoG38-128-13-22.

Calonne, N., C. Geindreau, F. Flin, S. Morin, B. Lesaffre, S. Rolland du Roscoat, and P. Charrier (2012), 3-D image-based numerical computations of snow permeability: Links to specific surface area, density, and microstructural anisotropy, *Cryosphere*, *6*(5), 939–951, doi:10.5194/tc-6-939-2012.

Colbeck, S. C. (1973), Theory of metamorphism of wet snow, research report 313, Cold Reg. Res. and Eng. Lab., Hanover, N. H.

Colbeck, S. C. (1979), Grain clusters in wet snow, *J. Colloid Interface Sci.*, *72*, 371–384, doi:10.1016/0021-9797(79)90340-0.

Colbeck, S. C. (1980), Thermodynamics of snow metamorphism due to variations in curvature, *J. Glaciol.*, *26*, 291–301.

Colbeck, S. C. (1982), An overview of seasonal snow metamorphism, *Rev. Geophys. Space Phys.*, *20*, 45–61.

Colbeck, S. C. (1986a), Statistics of coarsening in water - saturated snow, *Acta Metall.*, *34*(3), 347–352, doi:10.1016/0001-6160(86)90070-2.

Colbeck, S. C. (1986b), Classification of seasonal snow cover crystals, *Water Resour. Res.*, *22*(9), 59S–70S, doi:10.1029/WR022i09Sp0059S.

Denoth, A. (1994), An electronical device for long-term snow wetness recording, *Ann. Glaciol.*, *19*, 104–106, doi:10.1016/0148-9062(95)90311-R.

Dietz, A. J., C. Kuenzer, U. Gessner, and S. Dech (2012), Remote sensing of snow—A review of available methods, *Int. J. Remote Sens.*, *33*(13), 4094–4134, doi:10.1080/01431161.2011.640964.

Fierz, C., R. Armstrong, Y. Durand, P. Etchevers, E. Greene, D. McClung, K. Nishimura, P. Satyawali, and S. Sokratov (2009), The international classification for seasonal snow on the ground, *IHP-VII Tech. Doc. Hydrol. 83*, IACS Contrib. 1, UNESCO - IHP, Paris.

Hagenmuller, P., G. Chambon, F. Flin, S. Morin, and M. Naaim (2014), Snow as a granular material: Assessment of a new grain segmentation algorithm, *Granular Matter*, *16*, 421–432, doi:10.1007/s10035-014-0503-7.

Hagenmuller, P., M. Matzl, G. Chambon, and M. Schneebeli (2016), Sensitivity of snow density and specific surface area measured by microtomography to different image processing algorithms, *Cryosphere*, *10*(3), 1039–1054, doi:10.5194/tc-10-1039-2016.

Hildebrand, T., and P. Rüegsegger (1997), A new method for the model-independent assessment of thickness in three-dimensional images, *J. Microsc.*, *185*(1), 67–75, doi:10.1046/j.1365-2818.1997.1340694.x.

Hirashima, H., S. Yamaguchi, and T. Katsushima (2014), A multi-dimensional water transport model to reproduce preferential flow in the snowpack, *Cold Reg. Sci. Technol.*, *108*, 80–90, doi:10.1016/j.coldregions.2014.09.004.

Illangasekare, T. H., R. J. Walter Jr., M. F. Meier, and W. T. Pfeffer (1990), Modeling of meltwater infiltration in subfreezing snow, *Water Resour. Res.*, *26*(5), 1001–1012, doi:10.1029/WR026i005p01001.

Kaempfer, T. U., and M. Schneebeli (2007), Observation of isothermal metamorphism of new snow and interpretation as a sintering process, *J. Geophys. Res.*, *112*, D24101, doi:10.1029/2007JD009047.

Katsushima, T., S. Yamaguchi, T. Kumakura, and A. Sato (2013), Experimental analysis of preferential flow in dry snowpack, *Cold Reg. Sci. Technol.*, *85*, 206–216, doi:10.1016/j.coldregions.2012.09.012.

Kattelmann, R. (1985), Macropores in snowpacks of Sierra Nevada, *Ann. Glaciol.*, *6*, 272–273.

Kinar, N. J., and J. W. Pomeroy (2015), Measurement of the physical properties of the snowpack, *Rev. Geophys.*, *53*, 1–64, doi:10.1002/2015RG000481.

Kottegoda, N. T., and R. Rosso (2008), *Applied Statistics for Civil and Environmental Engineers*, McGraw-Hill, New York.

Löwe, H., J. K. Spiegel, and M. Schneebeli (2011), Interfacial and structural relaxations of snow under isothermal conditions, *J. Glaciol.*, *57*, 499–510, doi:10.3189/002214311796905569.

Marsh, P. (1987), Grain growth in a wet arctic snow cover, *Cold Reg. Sci. Technol.*, *14*, 23–31, doi:10.1016/0165-232X(87)90041-3.

Marsh, P., and M.-K. Woo (1984a), Wetting front advance and freezing of meltwater within a snow cover: 1. Observations in the Canadian Arctic, *Water Resour. Res.*, *20*(12), 1853–1864, doi:10.1029/WR020i012p01853.

Marsh, P., and M.-K. Woo (1984b), Wetting front advance and freezing of meltwater within a snow cover: 2. A simulation model, *Water Resour. Res.*, *20*(12), 1865–1874, doi:10.1029/WR020i012p01865.

Marsh, P., and M.-K. Woo (1985), Meltwater movement in natural heterogeneous snow covers, *Water Resour. Res.*, *21*(11), 1710–1716, doi:10.1029/WR021i011p01710.

McGurk, B. J., and P. Marsh (1995), Flow-finger continuity in serial thick-sections in a melting Sierran snowpack, in *Blogeochemistry of Seasonally Snow-Covered Catchments*, Proceedings of a Boulder Symposium, July 1995. IAHS Publ., *228*, 81–88.

Mitterer, C., H. Hirashima, and J. Schweizer (2011), Wet-snow instabilities: comparison of measured and modelled liquid water content and snow stratigraphy, *Ann. Glaciol.*, *52*(58), 201–208, doi:10.3189/172756411797252077.

Obbard, R. W. (2015), X-ray computed microtomography of sea ice—Comment on "A review of air-ice chemical and physical interactions (AICI): liquids, quasi-liquids, and solids in snow" by Bartels-Rausch et al. (2014), *Atmos. Chem. Phys.*, *15*(14), 8457–8458, doi:10.5194/acp-15-8457-2015.

Obbard, R. W., G. Troderman, and I. Baker (2009), Imaging brine and air inclusions in sea ice using micro-X-ray computed tomography, *J. Glaciol.*, *55*(194), 1113–1115.

Pfeffer, W. T., and N. F. Humphrey (1996), Determination of timing and location of water movement and ice-layer formation by temperature measurements in sub-freezing snow, *J. Glaciol.*, *42*(141), 292–304, doi:10.3198/1996JoG42-141-292-304.

Pfeffer, W. T., T. H. Illangasekare, and M. F. Meier (1990), Analysis and modeling of melt-water refreezing in dry snow, *J. Glaciol.*, *36*(123), 238–246, doi:10.3198/1990JoG36-123-238-246.

Pfeffer, W. T., M. F. Meier, and T. H. Illangasekare (1991), Retention of Greenland runoff by refreezing: Implications for projected future sea level change, *J. Geophys. Res.*, *96*(22), 22,117–22,124, doi:10.1029/91JC02502.

Pinzer, B. R., and M. Schneebeli (2009), Snow metamorphism under alternating temperature gradients: Morphology and recrystallization in surface snow, *Geophys. Res. Lett.*, *36*, L23503, doi:10.1029/2009GL039618.

Pinzer, B. R., A. Medebach, H. J. Limbach, C. Dubois, M. Stampanoni, and M. Schneebeli (2012), 3D-characterization of three-phase systems using X-ray tomography: Tracking the microstructural evolution in ice cream, *Soft Matter*, *8*, 4584–4594.

Raymond, C. F., and K. Tusima (1979), Grain coarsening of water-saturated snow, *J. Glaciol.*, *22*, 83–105.

Schleef, S., and H. Löwe (2013), X-ray microtomography analysis of isothermal densification of new snow under external mechanical stress, *J. Glaciol.*, *59*, 233–243.

Schleef, S., M. Jaggi, H. Löwe, and M. Schneebeli (2014), An improved machine to produce nature-identical snow in the laboratory, *J. Glaciol.*, *60*(219), 94–102, doi:10.3189/2014JoG13J118.
Schneebeli, M. (1995), Development and stability of preferential flow paths in a layered snowpack, in *Blogeochemistry of Seasonally Snow-Covered Catchments*, *IAHS Publ.*, *228*, 89–95.
Schweizer, J., J. B. Jamieson, and M. Schneebeli (2003), Snow avalanche formation, *Rev. Geophys.*, *41*(4), 1016, doi:10.1029/2002RG000123.
Techel, F., and C. Pielmeier (2011), Point observations of liquid water content in wet snow—Investigating methodical, spatial and temporal aspects, *Cryosphere*, *5*(2), 405–418, doi:10.5194/tc-5-405-2011.
Tedesco, M., E. J. Kim, A. W. England, R. D. De Roo, and J. P. Hardy (2006), Brightness temperatures of snow melting/refreezing cycles: Observations and modeling using a multilayer dense medium theory-based model, *IEEE Trans. Geosci. Remote Sens.*, *44*(12), 3563–3573, doi:10.1109/TGRS.2006.881759.
Tusima, K. (1985), Grain coarsening of snow particles immersed in water and solutions, *Ann. Glaciol.*, *6*, 126–129.
Wakahama, G. (1968), *The Metamorphism of Wet Snow*, Int. Assoc. of Sci. Hydrol. Publ., *79*, 458 pp.
Waldner, P. A., M. Schneebeli, U. Schultze-Zimmermann, and H. Flühler (2004), Effect of snow structure on water flow and solute transport, *Hydrol. Processes*, *18*(7), 1271–1290, doi:10.1002/hyp.1401.
Walter, B., S. Horender, C. Gromke, and M. Lehning (2013), Measurements of the pore-scale water flow through snow using fluorescent particle tracking velocimetry, *Water Resour. Res.*, *49*, 7448–7456, doi:10.1002/2013WR013960.
Wever, N., C. Fierz, C. Mitterer, H. Hirashima, and M. Lehning (2014), Solving Richards equation for snow improves snowpack meltwater runoff estimations in detailed multi-layer snowpack model, *Cryosphere*, *8*(1), 257–274, doi:10.5194/tc-8-257-2014.
Wever, N., C. Vera Valero, and C. Fierz (2016a), Assessing wet snow avalanche activity using detailed physics based snowpack simulations, *Geophys. Res. Lett.*, *43*, 5732–5740, doi:10.1002/2016GL068428.
Wever, N., S. Würzer, C. Fierz, and M. Lehning (2016b), Simulating ice layer formation under the presence of preferential flow in layered snowpacks, *Cryosphere*, *10*(6), 2731–2744, doi:10.5194/tc-10-2731-2016.
Williams, M. W., T. A. Erickson, and J. L. Petrzelka (2010), Visualizing meltwater flow through snow at the centimetre-to-metre scale using a snow guillotine, *Hydrol. Processes*, *24*, 2098–2110.
Yamaguchi, S., T. Katsushima, A. Sato, and T. Kumakura (2010), Water retention curve of snow with different grain sizes, *Cold Reg. Sci. Technol.*, *64*, 87–93, doi:10.1016/j.coldregions.2010.05.008.
Yamaguchi, S., K. Watanabe, T. Katsushima, A. Sato, and T. Kumakura (2012), Dependence of the water retention curve of snow on snow characteristics, *Ann. Glaciol.*, *53*(61), 6–12, doi:10.3189/2012AoG61A001.
Zermatten, E., S. Haussener, M. Schneebeli, and A. Steinfeld (2011), Tomography–based determination of permeability and Dupuit-Forchheimer coefficient of characteristic snow samples, *J. Glaciol.*, *57*(205), 811–816, doi:10.3189/002214311798043799.